A Digital Predistorter with Adaptive Architecture for High Efficient Envelope Tracking Power Amplifiers

Jiangnan Yuan, Chenwei Feng

***Abstract*—**Envelope tracking power amplifiers, though having high efficiency for non-constant envelope signals, also exhibit distinct "S" shape characteristics, which is very difficult to be compensated by employing traditional polynomial predistortion techniques. In order to deal with the problem, a universal digital predistorter of cascaded simplicial canonical piecewise linear function and memory polynomial model is proposed. The architecture of the proposed predistorter has "adaptive" capacity to varied power amplifiers. The complex separable least squares algorithm (CSLS) is presented for the parameters identification as well. Simulation demonstrated that the convergence speed and identification error of the CSLS algorithm are superior to those of least mean square type algorithms. The proposed predistorter model is effective on linearization of different types of envelope tracking power amplifiers, with an improvement of Adjacent Channel Power Ratio (ACPR) over 35dB.

***Keywords*—**digital predistorter, envelope tracking, SCPWL function, separable least squares, memory polynomial

I. Introduction

BASED on the state-of-the-art method of dynamic change of supply voltage, envelope tracking power amplifiers (ET PAs) can obtain over 60% power-added efficiency [1]-[3] in the case of non-constant envelope input signals. In order to carry out researches on predistortion techniques for ET PAs, we propose ET PA macro models with memory effects by cascading memory polynomial (MP) [4], linear time invariant (LTI) filter, Saleh and ET nonlinear models. Because of their operation principle, ET PAs exhibit distinct "S" shape nonlinear AM-AM characteristic, which will produce inband distortion, outband spectrum leakage and adjacent channel interference. And due to the special characteristics, ET PAs are unable to be compensated by the existing power series polynomial based digital predistorters (DPD) [5]. Simplicial canonical piecewise linear (SCPWL) function [6], [7] is a new simple piecewise approximation approach which is easy for hardware implementation. The merits of SCPWL and MP models will be exploited by cascading both of them. Therefore, we introduce SCPWL and MP cascaded model to construct a universal DPD in this paper. And the architecture of the proposed DPD is able to adapt to ET and other types of PAs.

Parameters identification of cascaded model has always been a difficult problem. Common algorithms include the Filter-x least mean square (LMS) algorithm [8] and the dual-loop LMS algorithm recently proposed in [6]. However, due to data correlations, the convergence speed of LMS-type algorithms is slow, and the result of parameters estimation is biased. What's more, it's necessary for ET PAs to be compensated both in large and small power regions. The DPD needs more parameters, and the identification accuracy of LMS-type algorithms is seriously deteriorated. The separable least squares (SLS) algorithm [9], [10] is a Newton-type algorithm commonly used in cascade model identification. However, to the best of the authors' knowledge, the SLS algorithm is limited in real number field, and cannot meet the requirements of complex data. Therefore, we propose the complex SLS (CSLS) algorithm for the cascaded piecewise DPD parameters identification.

The rest of the paper is organized as follows. In Section II, we describe the system architecture and the PA model. Then, Section III presents the complex Levenberg Marquardt (LM) algorithm, which is essential to the CSLS algorithm. Section IV proposes the CSLS algorithm and its application details in the DPD parameters identification, and the hardware structure of the DPD is also presented. Section V validates the performances of the proposed algorithm and the DPD. Finally, Section VI includes the conclusions of the paper.

II. System Architecture and Model

A. ET PA Model

So far, there has been short of any commercialized objects and even simulation models for ET PAs, which makes it inconvenient for the urgent need of research work at present. The structure of ET PAs is shown in Fig. 1. As can be seen from the figure, the power source of the radio frequency (RF) main amplifier is fed dynamically through the amplification version of the signal envelope. As a result, the main RF amplifier always

This research was supported by 2015 Natural Science Foundation of Fujian Province of China under Grant 2015J01670, 2015 Science and Technology Planning Project of Xiamen under Grant 3502Z20153017 and 2014 Research Foundation for Advanced Talents, Xiamen University of Technology under Grant YKJ14008R.

Jiangnan Yuan is with the School of Photoelectricity and Communication Engineering, Xiamen University of Technology, Xiamen, China (corresponding author to provide e-mail: jnyuan@xmut.edu.cn).

Chenwei Feng is with the School of Photoelectricity and Communication Engineering, Xiamen University of Technology, Xiamen, China (e-mail: cwfeng@xmut.edu.cn).

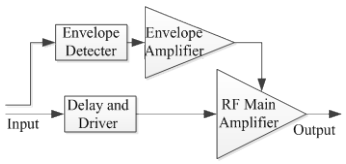

Fig. 1 Structure of ET PAs

operates near the saturation region [11], which enables it to achieve a very high efficiency. However, when the input signal envelope is small, the gain of the output transistor decreases because of the low supply voltage, which results in a reverse bend of the characteristic curve in the small power region. At the same time, the curve still bends in the large power saturation region, and the whole curve shows a distinct "S" shape [5]. Recently, Draxler *et al*. proposed a function to fit the curve in the small power region [12]:

$$y(n) = \max(y(n)) \left(\frac{\left(|z(n)| + b \cdot e^{-\frac{|z(n)|}{b}} \right)}{\left(1 + b \cdot e^{-\frac{1}{b}} \right)} - \frac{b}{1 + b \cdot e^{-\frac{1}{b}}} \right) \quad (1)$$

where b is a factor to control bending, generally taken from 0.01 to 0.1. For brevity, we name (1) "ET" model. Cascading method is commonly used to construct nonlinear models with memory effects, e.g., Hammerstein and Wiener models [9]. We propose two types of ET PA models. MP-ET model is constructed by cascading memory nonlinear MP and ET models. LTI-Saleh-ET model is constructed with the combination of LTI filter, Saleh [13] and ET models. The proposed ET PA models include most of the practical PA models currently.

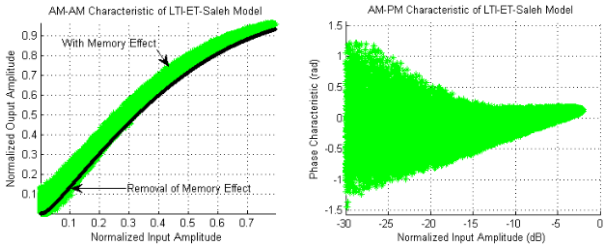

Fig. 2 AM-AM and AM-PM characteristics of the LTI-Saleh-ET PA

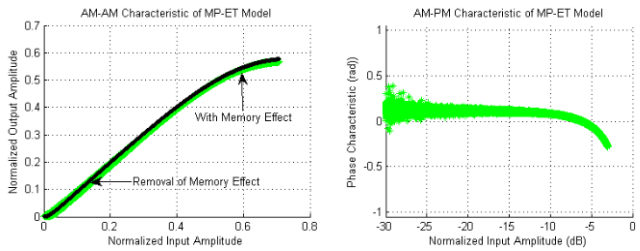

Fig. 3 AM-AM and AM-PM characteristics of the MP-ET PA

The AM-AM and AM-PM characteristics of the proposed models are shown in Fig. 2-3 respectively, wherein $b = 0.03$. For clarity, the figures also show the curves with the removal of memory effects. The reverse bending characteristics can be clearly seen in the small power region. The unique characteristics of ET come from various causes, e.g. the non-ideality of the envelope amplifier. In order to focus on the nonlinear compensation problem, the method we use is to "pack" all the non-idealities into the proposed ET PA macro model.

B. Predistortion System Architecture

We propose a DPD structure with cascaded SCPWL and MP model, as shown in Fig. 4. The proposed structure endows the DPD with an adaptive capacity to different types of PAs as follows:

a) SCPWL function is essential to the compensation of reverse bending characteristic of ET and other hard nonlinear models.
b) MP model DPD can compensate MP amplifiers. If the PA model is LTI-Saleh-ET, the DPD's MP part degrades to a linear FIR filter.
c) Not only the PA models proposed in this paper, but also other hard nonlinear PA models may be compensated by the proposed DPD.
d) The DPD model will be adjusted automatically in the process of parameters identification according to the responses of PAs.

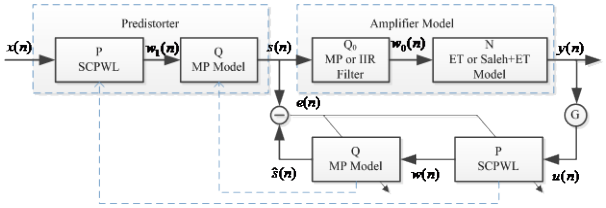

Fig. 4 Architecture of the predistortion system

The system uses the efficient indirect learning structure [2], as shown in Fig. 4. In order to describe deeper memory characteristics, in LTI-Saleh-ET PA model, infinite impulse response (IIR) filter is used. The transfer function of IIR filter, the characteristics of Saleh and MP model are shown in (2) to (4) respectively as follows:

$$H(z) = \frac{b_0 + b_1 z^{-1} + b_2 z^{-2}}{1 + a_1 z^{-1} + a_2 z^{-2}} \quad (2)$$

$$A_{PA} = \frac{\alpha_1 r}{1 + \alpha_2 r^2}; \varphi_{PA} = \frac{\eta_1 r^2}{1 + \eta_2 r^2} \quad (3)$$

$$y(n) = \sum_{l=1, l \in odd}^{L} \sum_{r=0}^{R-1} a_{lr} s(n-r) |s(n-r)|^{l-1} \quad (4)$$

where r is the amplitude of input signals, b_0, b_1, b_2, a_1, a_2, α_1, α_2, η_1, η_2, a_{lr} are model parameters.

C. SCPWL Function

SCPWL function is a piecewise linear interpolation function employing the absolute value function, whose base functions are [6], [7]:

$$\lambda_i(x)=\begin{cases}\frac{1}{2}(x-\beta_i+|x-\beta_i|), & x<\beta_S\\ \frac{1}{2}(\beta_S-\beta_i+|\beta_S-\beta_i|), & x\geq\beta_S\end{cases} \quad i=1,2,...S-1 \quad (5)$$

where x, $\lambda_i(x)$, β_i, and β_s are the input, output, break point and saturation point respectively. S is the number of segments. The total output can be denoted as $f(x)=\boldsymbol{\lambda}(x)^{\mathrm{T}}\boldsymbol{c}$, where $\boldsymbol{\lambda}(x)$ and $\boldsymbol{c}$ are base function and coefficient vector respectively.

III. LM Algorithm in Complex Number Field

The Levenberg Marquardt (LM) algorithm is a common optimization algorithm in real number field, and it is essential to the CSLS algorithm. In this paper, the LM algorithm needs to be extended to the complex number field. We follow the Wirtinger Calculus derivative rules [14] for nonanalytic real functions $f(z,z^*)$ with complex input variables (z,z^*), i.e. when $f(z,z^*)$ differentiates with respect to z, z^* will be treated as constant and vice versa.

By using the Taylor series expansion of $f(\boldsymbol{z},\boldsymbol{z}^*), f\in R,\boldsymbol{z}\in C^N$, let $\boldsymbol{a}=\frac{\partial f(\boldsymbol{z},\boldsymbol{z}^*)}{\partial \boldsymbol{z}}$, $\boldsymbol{v}=(\boldsymbol{z}-\boldsymbol{z}_0)$ $\boldsymbol{A}=\frac{\partial^2 f(\boldsymbol{z}_0,\boldsymbol{z}_0^*)}{\partial \boldsymbol{z}\partial \boldsymbol{z}^{\mathrm{T}}}$, $\boldsymbol{B}=\frac{\partial^2 f(\boldsymbol{z}_0,\boldsymbol{z}_0^*)}{\partial \boldsymbol{z}\partial \boldsymbol{z}^{\mathrm{H}}}$, we can find that the $\boldsymbol{v}$ being able to bring a maximum amount of change on $f(\boldsymbol{z},\boldsymbol{z}^*)$ [15] is:

$$\boldsymbol{v}=\left(\boldsymbol{B}^*-\boldsymbol{A}^*\boldsymbol{B}^{-1}\boldsymbol{A}\right)^{-1}\left(\boldsymbol{A}^*\boldsymbol{B}^{-1}\boldsymbol{a}-\boldsymbol{a}^*\right) \quad (6)$$

In system identification applications, the cost function is usually set to $\varepsilon=\sum_{i=1}^{N}|e(n)|^2$, where $e(n)=y(n)-\boldsymbol{z}^{\mathrm{T}}\boldsymbol{x}(n)$, $y(n)$, $\boldsymbol{x}(n)$ and $\boldsymbol{z}$ are output error, reference, input vector and parameters vector under identification. Let $\boldsymbol{e}=[e(1),e(2),...,e(N)]^{\mathrm{T}}$, then $\varepsilon=f(\boldsymbol{e},\boldsymbol{e}^*)=\boldsymbol{e}^{\mathrm{H}}\boldsymbol{e}$ is the real function of complex vector $\boldsymbol{e}$, and thus we obtain the following first derivatives:

$$\begin{aligned}&\frac{\partial f(\boldsymbol{e},\boldsymbol{e}^*)}{\partial \boldsymbol{z}}=\boldsymbol{J}^{\mathrm{T}}\boldsymbol{e}^*,\frac{\partial f(\boldsymbol{e},\boldsymbol{e}^*)}{\partial \boldsymbol{z}^{\mathrm{T}}}=\boldsymbol{e}^{\mathrm{H}}\boldsymbol{J}\\ &\frac{\partial f(\boldsymbol{e},\boldsymbol{e}^*)}{\partial \boldsymbol{z}^*}=\boldsymbol{J}^{\mathrm{H}}\boldsymbol{e},\frac{\partial f(\boldsymbol{e},\boldsymbol{e}^*)}{\partial \boldsymbol{z}^{\mathrm{H}}}=\boldsymbol{e}^{\mathrm{T}}\boldsymbol{J}^*\end{aligned} \quad (7)$$

where 'T', 'H' and '*' denote transpose, hermitian transpose and complex conjugate respectively. In (7), $\boldsymbol{J}$ is the complex Jacobian matrix of $\boldsymbol{e}$ with respect to $\boldsymbol{z}$. And the second derivatives are:

$$\begin{aligned}&\frac{\partial^2 f(\boldsymbol{e},\boldsymbol{e}^*)}{\partial \boldsymbol{z}\partial \boldsymbol{z}^{\mathrm{T}}}=\frac{\partial^2 f(\boldsymbol{e},\boldsymbol{e}^*)}{\partial \boldsymbol{z}^*\partial \boldsymbol{z}^{\mathrm{H}}}=\boldsymbol{0}\\ &\frac{\partial^2 f(\boldsymbol{e},\boldsymbol{e}^*)}{\partial \boldsymbol{z}^*\partial \boldsymbol{z}^{\mathrm{T}}}=\boldsymbol{J}^{\mathrm{H}}\boldsymbol{J},\frac{\partial^2 f(\boldsymbol{e},\boldsymbol{e}^*)}{\partial \boldsymbol{z}\partial \boldsymbol{z}^{\mathrm{H}}}=\boldsymbol{J}^{\mathrm{T}}\boldsymbol{J}^*\end{aligned} \quad (8)$$

Using (7)-(8) in (6), we have $\boldsymbol{v}=-\left(\boldsymbol{J}^{\mathrm{H}}\boldsymbol{J}\right)^{-1}\boldsymbol{J}^{\mathrm{H}}\boldsymbol{e}$. Finally, the update equation of $\boldsymbol{z}$ which brings the steepest descent to the cost function is:

$$\boldsymbol{z}=\boldsymbol{z}_0-\left(\boldsymbol{J}^{\mathrm{H}}\boldsymbol{J}\right)^{-1}\boldsymbol{J}^{\mathrm{H}}\boldsymbol{e} \quad (9)$$

Equation (9) can be looked as the generalization of Gauss-Newton algorithm in the complex field. Compared with LMS-type algorithms, it has the advantages of fast convergence, without being affected by data correlations. Its main disadvantage is that if $\boldsymbol{J}$ is rank deficient or nearly rank deficient, (9) will be numerically instable. Similarly to the LM algorithm in real number field [16], we use a variable regular factor to solve this problem, and correct the Hessian Matrix of the algorithm to $\left(\boldsymbol{J}^{\mathrm{H}}\boldsymbol{J}+\delta\boldsymbol{I}\right)$, wherein δ being a small real factor. Finally, update equation of the complex LM algorithm can be summed up as:

$$\boldsymbol{z}=\boldsymbol{z}_0-\left(\boldsymbol{J}^{\mathrm{H}}\boldsymbol{J}+\delta\boldsymbol{I}\right)^{-1}\boldsymbol{J}^{\mathrm{H}}\boldsymbol{e} \quad (10)$$

IV. Complex Separable Least Squares Algorithm

In the feedback channel of Fig. 4, the output of part P is a function of the signal amplitude $|u(n)|$, which can be piecewise approximated by means of SCPWL function. Let the DPD's coefficient vectors of MP and SCPWL parts be $\boldsymbol{b}=[b_{10},b_{11},...,b_{1,M-1},b_{30},...,b_{K,M-1}]$ and $\boldsymbol{c}=[c_0,c_1,...,c_{S-1}]$, the outputs of the feedback channel be $\hat{s}(n)$ and $w(n)$ respectively, then we have

$$\begin{cases}\hat{s}(n)=\sum\limits_{k=1,k\in odd}^{K}\sum\limits_{m=0}^{M-1}b_{km}^*w(n-m)|w(n-m)|^{k-1}\\ w(n)=\sum\limits_{i=0}^{S-1}c_i\lambda_i\left(|u(n)|\right)u(n)\end{cases} \quad (11)$$

where M and K are the memory depth and orders of the MP part of the DPD respectively. S is the number of segments of the SCPWL part. Let $e(n)=s(n)-\hat{s}(n)$, cost function be $\varepsilon_N=\frac{1}{N}\sum_{n=1}^{N}|e(n)|^2$, define $\boldsymbol{\theta}\boldsymbol{b}=\{c \mid \}$, the coefficients

identification problem can be expressed as:

$$\hat{\boldsymbol{\theta}} = \arg\min_{\boldsymbol{\theta}} \varepsilon_N(\boldsymbol{\theta}) \tag{12}$$

Let the complex Jacobian matrix of $\boldsymbol{e} = [e(1),...,e(N)]$ with respect to $\boldsymbol{\theta}$ be $\boldsymbol{J} = \{\boldsymbol{J}_l \ | \boldsymbol{J}_n\}$, where $\boldsymbol{J}_l$ and $\boldsymbol{J}_n$ denote the linear and nonlinear complex Jacobian matrix respectively. The projection matrix of $\boldsymbol{J}_l$ is $\boldsymbol{P}_l = \boldsymbol{J}_l \left(\boldsymbol{J}_l^{\mathrm{H}} \boldsymbol{J}_l\right)^{-1} \boldsymbol{J}_l^{\mathrm{H}}$. When the system converges to the steady state, if there is a slight change $\boldsymbol{\delta}_n$ of the nonlinear part, the output of the feedback channel is $\hat{\boldsymbol{s}}(\boldsymbol{c}+\boldsymbol{\delta}_n) \approx \hat{\boldsymbol{s}}(\boldsymbol{c}) + \boldsymbol{J}_n \boldsymbol{\delta}_n$. Since the nonlinear parameters have changed, the linear parameters will no longer be optimal. We can find the optimal linear parameters again via a projection approximation method including two steps [9]. Step 1: project the change of the nonlinear part to the column space of $\boldsymbol{J}_l$. Step 2: let the linear part generate an opposite change $\boldsymbol{\delta}_l$ against the projection in order to achieve an optimization match again, i.e. $\boldsymbol{J}_l \boldsymbol{\delta}_l + \boldsymbol{P}_l \boldsymbol{J}_n \boldsymbol{\delta}_n = \boldsymbol{0}$. Therefore, we have

$$\hat{\boldsymbol{s}}(\boldsymbol{c}+\boldsymbol{\delta}_n) \approx \hat{\boldsymbol{s}}(\boldsymbol{c}) + \left(\boldsymbol{I} - \boldsymbol{P}_l\right) \boldsymbol{J}_n \boldsymbol{\delta}_n \tag{13}$$

Equation (13) maps the change of the linear part to the column space of the nonlinear part by means of the projection method. And now, we can treat the output $\hat{\boldsymbol{s}}(\boldsymbol{c})$ as a single input function of $\boldsymbol{\delta}_n$, and thus we have $\frac{\partial \hat{\boldsymbol{s}}}{\partial \boldsymbol{\delta}_n} = \left(\boldsymbol{I} - \boldsymbol{P}_l\right) \boldsymbol{J}_n$. Let $\boldsymbol{J}_t = \left(\boldsymbol{I} - \boldsymbol{P}_l\right) \boldsymbol{J}_n$, the amount of the change of $\boldsymbol{c}$ be $\Delta \boldsymbol{c} = \left(\boldsymbol{J}_t^{\mathrm{H}} \boldsymbol{J}_t + \delta \boldsymbol{I}\right)^{-1} \boldsymbol{J}_t^{\mathrm{H}} \boldsymbol{e}$, then the iterative update equation of $\boldsymbol{c}$ is:

$$\boldsymbol{c}(n+1) = \boldsymbol{c}(n) - \left(\boldsymbol{J}_t^{\mathrm{H}} \boldsymbol{J}_t + \delta \boldsymbol{I}\right)^{-1} \boldsymbol{J}_t^{\mathrm{H}} \boldsymbol{e} \tag{14}$$

Each time after the update of the coefficients of the SCPWL part, the coefficients of the MP part can be obtained through LS method. The calculation of $\boldsymbol{J}_t$ needs complex Jacobian matrix $\boldsymbol{J}_l$ and $\boldsymbol{J}_n$. We obtain the element $(n, \frac{k+1}{2} + m \cdot \frac{K+1}{2})$ of $\boldsymbol{J}_l$ by using (11) and the definition of $\boldsymbol{e}(n)$ as follows:

$$\frac{\partial e(n)}{\partial b_{km}} = -\frac{\partial \hat{s}(n)}{\partial b_{km}} = -w(n-m)\left|w(n-m)\right|^{k-1} \tag{15}$$

where $n = 1,2...,N$, $k = 1,3,...,K$, $m = 0,1...,M-1$. And the element $(n, i+1)$ of $\boldsymbol{J}_n$ is:

$$\begin{aligned} \frac{\partial e(n)}{\partial c_i} &= -\frac{\partial \hat{s}(n)}{\partial w(n-m)} \frac{\partial w(n-m)}{\partial c_i} \\ &= -\sum_{m=0}^{M-1} \sum_{\substack{k=1, \\ k \in odd}}^{K} \frac{k+1}{2} b_{km} \left|w(n-m)\right|^{k-1} \lambda_i\left(\left|u(n-m)\right|\right) u(n-m) \end{aligned} \tag{16}$$

where $i = 0,1...,S-1$.

If the parameters of the SCPWL and MP parts are multiplied by a same constant, the output will remain unchanged. Therefore, the first coefficient of $\boldsymbol{c}$ or $\boldsymbol{b}$ need to be normalized in each iteration. The flow chart of the CSLS algorithm is shown in Fig. 5, where the main control factors are the regular factor δ and reduction factor γ. During the iterative process, δ gradually reduces from its initial value and the convergence speed increases, with the decreasing of the error.

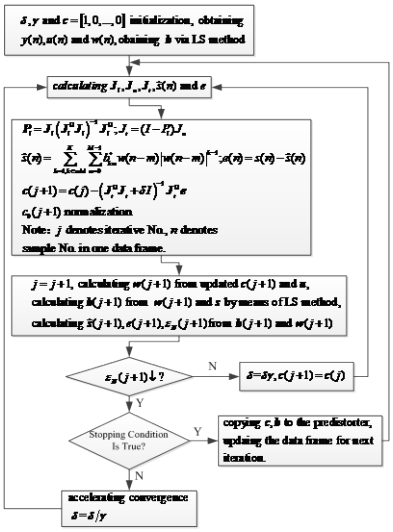

Fig. 5 Flow chart of the CSLS algorithm

V. Simulation Results and Discussion

In order to verify the effectiveness of the DPD and the identification algorithms, the performances of LMS-type and the CSLS algorithms, the outband spectrum leakage and the AM-AM and AM-PM characteristic curves of the PAs before and after predistortion are compared respectively. Simulation stimulus data are the 4-carrier WCDMA signal of 3GPP TS251.141 Test Model 1 with bandwidth of 20MHz. In MP-ET PA model, the MP parameters are set as follows:

$$\begin{aligned} &a_{10} = 1.0513 + 0.0904i; a_{11} = -0.0680 - 0.0023i; \\ &a_{12} = 0.0289 - 0.0054i; a_{30} = -0.0542 - 0.2900i; \\ &a_{31} = 0.2234 + 0.2317i; a_{32} = -0.0621 - 0.0932i; \\ &a_{50} = -0.9657 - 0.7028i; a_{51} = -0.2451 - 0.3735i \\ &a_{52} = 0.1229 + 0.1508i \end{aligned} \tag{17}$$

In LTI-Saleh-ET PA model, IIR transfer function parameters are set as $a_1 = 0.2$ $a_2 = 0$, $b_0 = 1$, $b_1 = 0$, $b_2 = 0.3$ and Saleh model parameters are set as the typical values of $\alpha_1 = 2.1587$,

$\alpha_2 = 1.1517$, $\eta_1 = 4.0033$, $\eta_2 = 9.1040$. ET model parameter is set as $b = 0.03$ for both types of PA models.

The identification algorithms include the dual-loop LMS [6], the Filter-x LMS [8] and the CSLS. Dual-loop LMS algorithm has two steps. Step 1 is to identify the parameter vector $\boldsymbol{a}$ of the MP part of the PA and the parameter vector $\boldsymbol{c}(n)$ of the SCPWL part of the DPD as shown in (18). If the PA is a LTI-Saleh-ET model, then vector $\boldsymbol{a}$ will degrade to a FIR filter's parameter vector which is approximate to the IIR filter of the PA model.

$$\begin{cases} a_{lr}(n+1) = a_{lr}(n) - \mu_1 e_0^*(n) w(n-r) \left| w(n-r) \right|^{l-1} \\ c_i(n+1) = c_i(n) + \mu_2 e_0^*(n) \lambda_i \left(\left| u(n) \right| \right) u(n) \end{cases} \tag{18}$$

where $l = 1,3,...,L$, $r = 0,1,...,R-1$, $i = 0,1,...,S-1$, R, L and S are the memory depth and orders of the MP part of the PA model and the number of segments of the DPD respectively. μ_1 and μ_2 are the step sizes.

In step 2 of the dual-loop LMS algorithm, $\boldsymbol{c}(n)$ will be copied directly into the SCPWL part of the DPD. Nevertheless $\boldsymbol{a}$ should be inversed to obtain the MP parameters $\boldsymbol{b}$ of the DPD:

$$\begin{cases} g(n) = e_1^*(n) \sum_{r=0}^{R-1} \dfrac{l+1}{2} \sum_{l=1, l\in odd}^{L} \left\{ a_{lr}^* s(n-r) \left| s(n-r) \right|^{l-1} \cdot \right. \\ \qquad \left. w_1(n-m-r) \left| w_1(n-m-r) \right|^{k-1} \right\} \\ b_{km}(n+1) = b_{km}(n) + \mu_3 g(n) \end{cases} \tag{19}$$

where $g(n)$ denotes the gradient of the LMS algorithm, μ_3 is the step size and $k = 1,3,...,K, m = 0,1,...,M-1$, K, M are order and memory depth of the DPD.

The Filter-x LMS algorithm uses LMS algorithm to update the coefficients of MP and SCPWL parts of the DPD simultaneously as follows:

$$\begin{cases} b_{km}(n+1) = b_{km}(n) + \mu_1 e^*(n) w(n-m) \left| w(n-m) \right|^{k-1} \\ c_i(n+1) = c_i(n) + \mu_2 e^*(n) \sum_{m=0}^{M-1} \sum_{k=1, k\in odd}^{K} \dfrac{1}{2} \left\{ (k+1) b_{km} \cdot \right. \\ \qquad \left. \left| w(n-m) \right|^{k-1} \lambda_i \left(\left| u(n-m) \right| \right) u(n-m) \right\} \end{cases} \tag{20}$$

where $k = 1,3,...,K$, $m = 0,1,...,M-1$, $i = 0,1,...,S-1$, μ_1 and μ_2 are the step sizes. In order to obtain a balance between the convergence speed and the identification accuracy, the step sizes of the dual-loop LMS algorithm are chosen as $\mu_1 = \mu_2 = \mu_3 = 0.1$, and the step sizes of the Filter-x LMS algorithm are chosen as $\mu_1 = \mu_2 = 0.1$. After simulation comparison, the CSLS algorithm parameters are chosen as $\delta = 1, \gamma = 5$.

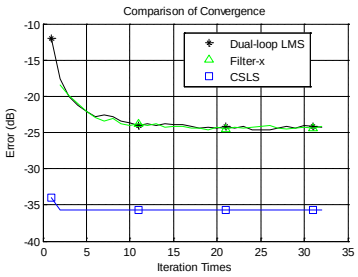

Fig. 6 Comparison of the convergence

Fig. 6 is the comparison of the convergence speed and error of three identification algorithms, where 1,024 samples are treated as one iteration time. The figure shows that the convergence speed and error of the dual-loop and the Filter-x LMS algorithm are almost the same. The CSLS algorithm comes to convergence only after a few iterations, with the error being better than the above two algorithms 10dB. It is because the CSLS is a Newton-type algorithm, which converges much faster than LMS-type algorithms, with estimation accuracy not being affected by data correlations.

Fig. 7 is the comparisons of the power spectrum density (PSD) of the LTI-Saleh-ET and MP-ET PAs after predistortion. The MP part of the DPD is set as $K = 5, M = 6$. The segments of SCPWL are set as $S = 12$ and $S = 10$ for LTI-ET-Saleh and MP-ET models respectively. The parameter numbers of the DPD are 28 and 30. As can be seen from the figure, the proposed DPD can compensate both types of PA models. Outband suppression effect of the DPD designed with the CSLS algorithm can be up to 35dB, far better than the two LMS-type algorithms. The reason is that the ET PA must be compensated in different power regions and the DPD needs more parameters, which results in strong data correlations. As a result, the performances of LMS-type algorithms drop more seriously.

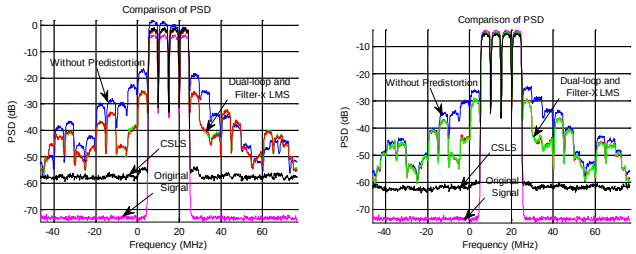

(a) LTI-Saleh-ET PA model (b) MP-ET PA model

Fig. 7 Comparisons of the PSD

Fig. 8 is the comparisons of the AM-AM characteristics of the LTI-Saleh-ET PA before and after predistortion with different identification algorithms. The characteristics of the DPD are also presented as well. Seen from the figure, the MP part of the DPD degrades to LTI filter automatically to compensate for the

memory effects of the PA. The AM-AM curve of the SCPWL part of the DPD in Fig. 8 (a) obviously bends in the small power region in order to compensate for the characteristics of the PA, while Fig. 8 (b) does not have this feature. Linearity and memory effects elimination of the PA after predistortion in Fig. 8 (a) are much better than in Fig. 8 (b). Fig. 9 is the comparisons of the AM-PM characteristics of the PA with different identification algorithms. From the comparisons, we can draw a conclusion that both the model of the DPD and the identification algorithms have impact on the effects of the linearization.

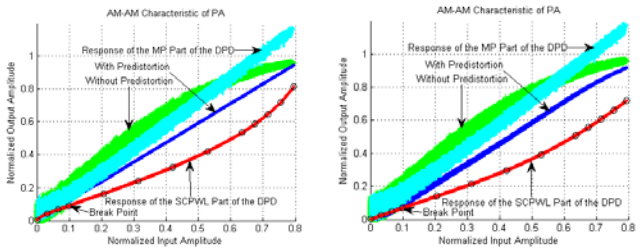

(a)With the CSLS algorithm (b)With the dual-loop LMS algorithm

Fig. 8 Comparisons of AM-AM characteristics of LTI-Saleh-ET PA after DPD with different identification algorithms

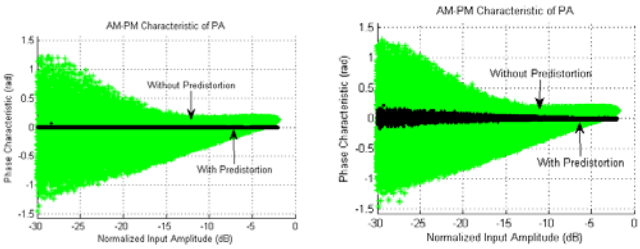

(a)With the CSLS algorithm (b)With the dual-loop LMS algorithm

Fig. 9 Comparisons of AM-PM characteristics of LTI-Saleh-ET PA after DPD with different identification algorithms

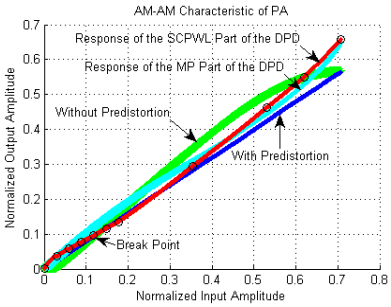

Fig. 10 AM-AM characteristic of MP-ET PA after DPD

Fig. 10 is the AM-AM characteristic curve of MP-ET PA. As can be seen from the figure, the SCPWL part compensates the reverse bending in small power region and part of the saturation nonlinearity, while the MP part is responsible for the compensation of memory effects and part of the saturation nonlinearity. Fig.11 is the AM-PM and normalized gain characteristics of the MP-ET PA. Seen from the figure, MP-ET PA has gain expansion and compression regions. Gain nonlinearity and dispersion phenomena are significantly improved after DPD compensation. From the simulation results of LTI-Saleh-ET and MP-ET PA models, a conclusion can be drawn that the proposed DPD of cascaded SCPWL and MP models has adaptive capacity to varied PA models.

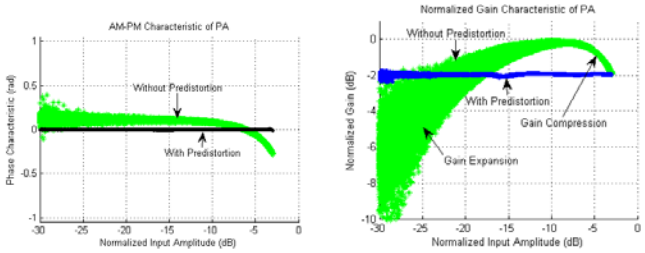

(a) AM-PM characteristic (b) Normalized gain characteristic

Fig. 11 AM-PM and normalized gain characteristics of MP-ET PA after DPD

VI. Conclusion

The proposed DPD structure has adaptive capacity to varied traditional and new-type PA models. With the cascaded architecture of SCPWL and MP, it can effectively compensate the strong nonlinear characteristics of ET PAs, with an ACPR improvement over 35dB. The performances of the CSLS algorithm are much better than those of LMS-type algorithms in convergence speed and identification accuracy. The algorithm also can be applied to other cascaded model, and thus provides a unified complex field identification algorithm for cascaded DPDs. SCPWL function has good prospects in engineering applications with the advantages of simple structure and easy hardware implementation. With the commercialization progress of ET PAs, further research directions include testing the performances of the proposed DPD on real ET PAs and applying the CSLS algorithms in other types of DPD models.

References

[1] G. T. Watkins and K. Mimis, "A 65% efficient envelope tracking radio-frequency power amplifier for orthogonal frequency division multiplex," *IET Microwaves, Antennas & Propagation*, vol. 9, no. 7, pp. 676-681, May 2015.

[2] S. Park, J. L. Woo, U. Kim and Y. Kwon, "Broadband CMOS Stacked RF Power Amplifier Using Reconfigurable Interstage Network for Wideband Envelope Tracking," *IEEE Tran. Microwave Theory and Techniques*, vol. 63, no. 4, pp. 1174-1185, April 2015.

[3] S. Jin, B. Park, K. Moon, J. Kim, M. Kwon, D. Kim and *et al.*, "A Highly Efficient CMOS Envelope Tracking Power Amplifier Using All Bias Node Controls," *IEEE Microwave and Wireless Components Letters*, vol. 25, no. 8, pp. 517-519, Aug. 2015.

[4] L. Ding, G. T. Zhou, D. R. Morgan, Z. X. Ma, and J. S. Kenney, "A robust digital baseband predistorter constructed using memory polynomials," *IEEE Trans. Communications*, vol.52, no.1, pp.159-165, Jan. 2004.

[5] A. Zhu, P. J. Draxler, C. Hsia, T. J. Brazil, D. F. Kimball and P. M. Asbeck, "Digital Predistortion for Envelope-Tracking Power Amplifiers Using Decomposed Piecewise Volterra Series," *IEEE Trans. Microwave Theory and Techniques*, vol.56, no. 10, pp. 2237-2247, Oct. 2008.

[6] M. Y. Cheong, S. Werner, M. J. Bruno, J. L. Figueroa, J. E. Cousseau and R. Wichman, "Adaptive Piecewise Linear Predistorters for Nonlinear Power Amplifiers With Memory," IEEE Trans. Circuits and Systems I: Regular Papers, vol.59, no.7, pp.1519-1532, July 2012.

[7] A. Zhu, "Decomposed Vector Rotation-Based Behavioral Modeling for Digital Predistortion of RF Power Amplifiers," *IEEE Trans. Microwave Theory and Techniques*, vol.63, no.2, pp.737-744, Feb. 2015.

[8] Y. H. Lim, Y. S. Cho, I. W. Cha and D. H. Youn, "An adaptive nonlinear prefilter for compensation of distortion in nonlinear systems," *IEEE Trans. Signal Processing*, vol.46, no.6, pp.1726-1730, June 1998.

[9] E. J. Dempsey and D. T. Westwick, "Identification of Hammerstein models with cubic spline nonlinearities," *IEEE Trans. Biomedical Engineering*, vol.51, no.2, pp.237-245, Feb. 2004.
[10] G. van der Veen, J. W. van Wingerden and M. Verhaegen, "Global Identification of Wind Turbines Using a Hammerstein Identification Method," *IEEE Trans. Control Systems Technology*, vol. 21, no.4, pp.1471-1478, July 2013.
[11] D. Kang, B. Park, D. Kim, J. Kim, Y. Cho and B. Kim, "Envelope-Tracking CMOS Power Amplifier Module for LTE Applications," *IEEE Transactions on Microwave Theory and Techniques*, vol. 61, no. 10, pp. 3763-3773, Oct. 2013.
[12] P. J. Draxler, J. J. Yan, D. F. Kimball and P. M. Asbeck, "Digital predistortion for envelope tracking power amplifiers," *in Proc. of 13th Conf. of 2012 IEEE Annual Wireless and Microwave Technology (WAMICON)*, pp.1-7, April 2012.
[13] A. A. M. Saleh, "Frequency-independent and frequency independent nonlinear models for TWT amplifiers," *IEEE Trans. Communications*, vol. 29, no.11, pp.1715-1720, Nov. 1981.
[14] N. Lashkarian, J. Shi and M. Forbes, "A Direct Learning Adaptive Scheme for Power-Amplifier Linearization Based on Wirtinger Calculus," *IEEE Trans. Circuits and Systems I: Regular Papers*, vol.61, no.12, pp.3496-3505, Dec. 2014.
[15] Guangrong Yan and F. H. Howard, "A Newton-like algorithm for complex variables with applications in blind equalization," *IEEE Trans. Signal Processing*, vol. 48, no.2, pp. 553-556, Feb. 2000.
[16] J. Nocedal and S. J. Wright, *Numerical Optimization, 2nd Edition*, Springer, New York, 2006, pp.258-261.

Jiangnan Yuan received the B.S and M.S. degrees in electronic engineering from Shanghai Jiaotong University and Xiamen University, China, in 1993 and 2004 respectively, and the Ph.D. degree in communication and information system from Xiamen University in 2013. He has worked for Xiamen University of Technology since 2004 and is currently an associate professor with the School of Photoelectricity and Communication Engineering. His research interests include adaptive signal processing, communication signal processing and its VLSI implementation and digital predistortion.

Chenwei Feng received the B.S and M.S. degree in communication and information system form Fuzhou University and Xiamen University, China, in 2004 and 2007 respectively. He is now pursuing Ph.D. degree in communication and information in Xiamen University. He has been in Xiamen University of Technology since 2007 and is currently an assistant professor with the School of Photoelectricity and Communication Engineering. His research interests include signal processing, cognitive radio networks and digital predistortion.